BEILSTEIN JOURNAL OF ORGANIC CHEMISTRY

Supporting Information

for

CO_2 silylation at a tucked-in iron(II) complex

Logan J. Taylor and Marcus W. Drover

Beilstein J. Org. Chem. **2026,** *22,* 1295–1302. doi:10.3762/bjoc.22.104

Copies of spectra and crystallography details

Table of contents

1. Spectroscopic data S2
2. Mass spectrometry S18
3. Crystallographic details S20
4. References S22

1. Spectroscopic data:

Figure S1: 2, ^{1}H NMR, C_6D_6, 400 MHz, 298 K.

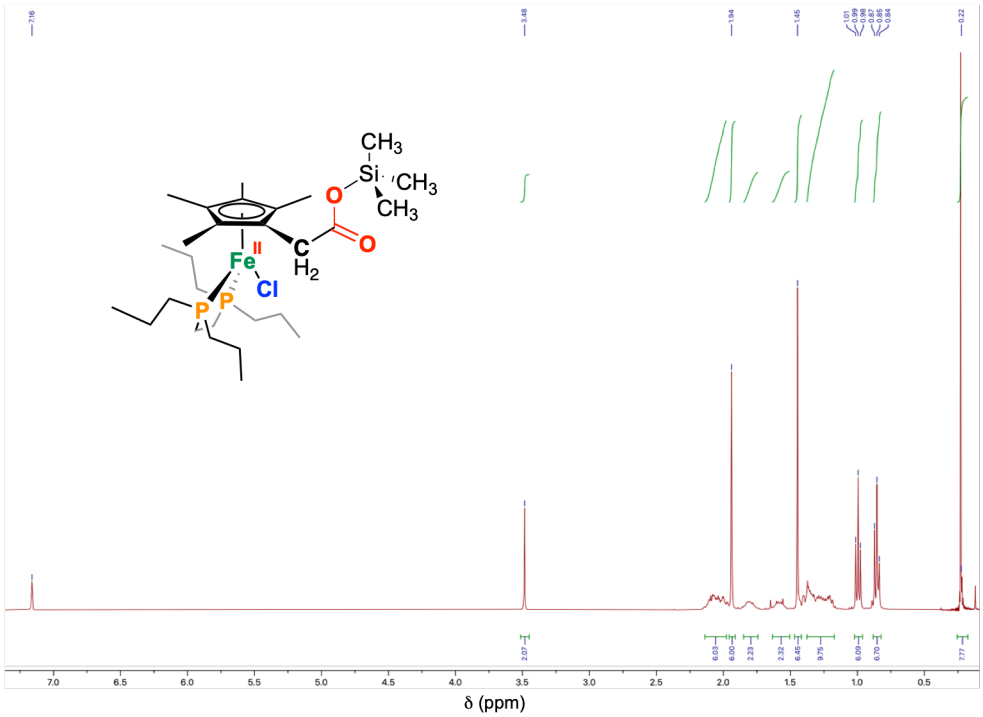

Figure S2: 2, $^{31}P\{^{1}H\}$ NMR, C_6D_6, 162 MHz, 298 K.

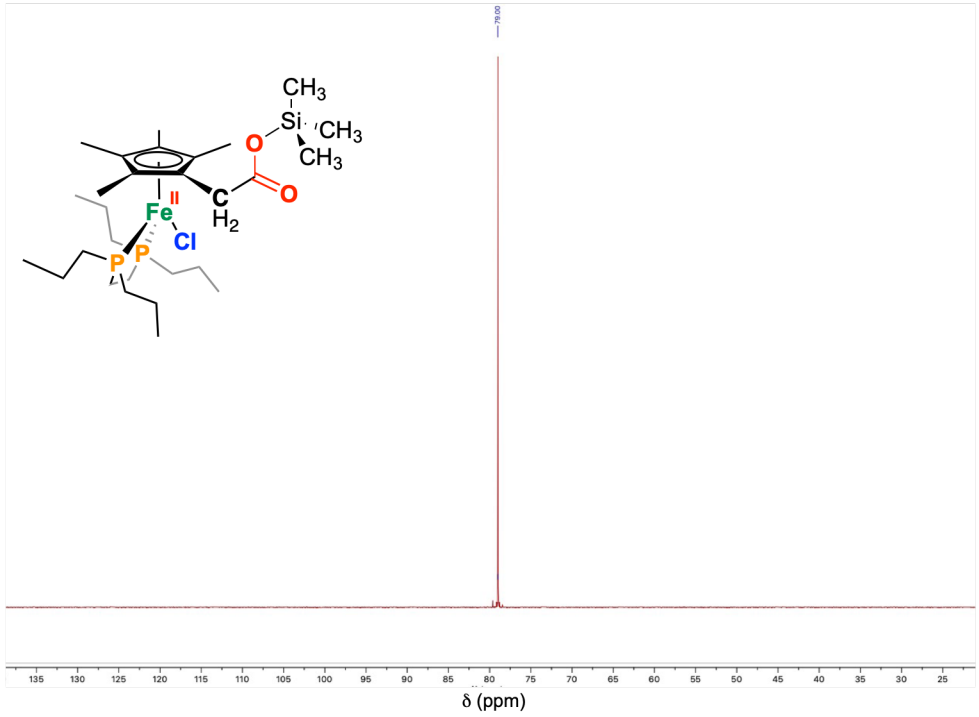

Figure S3: 2, $^{1}H,^{29}Si$ HMBC NMR, C_6D_6, 400 MHz, 298 K.

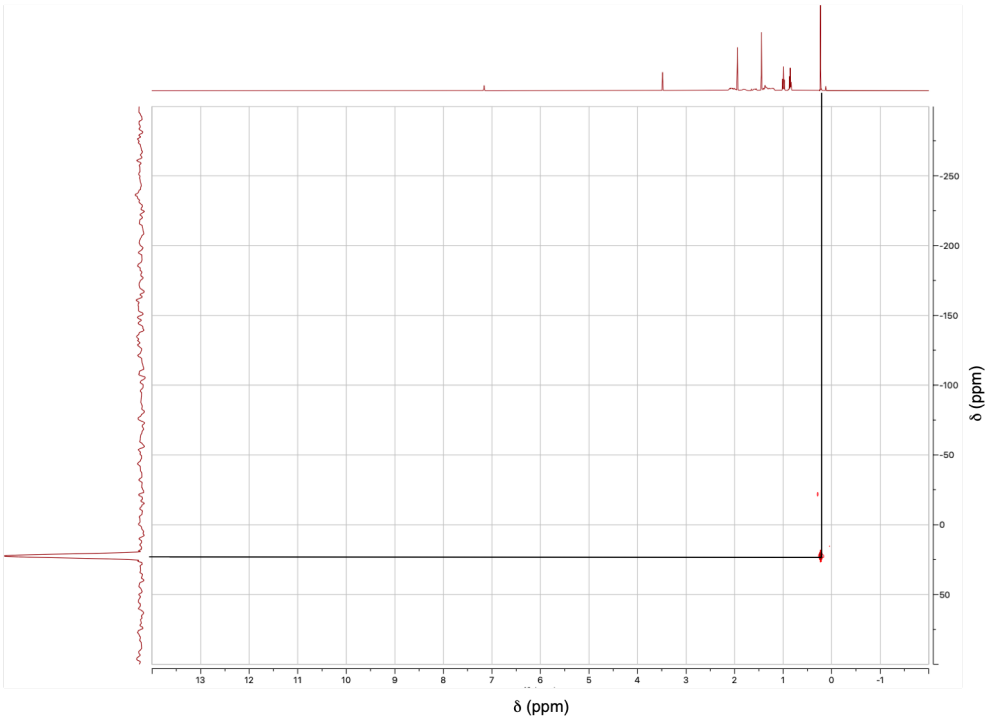

Figure S4: 2, $^{13}C\{^{1}H\}$ NMR, C_6D_6, 101 MHz, 298 K.

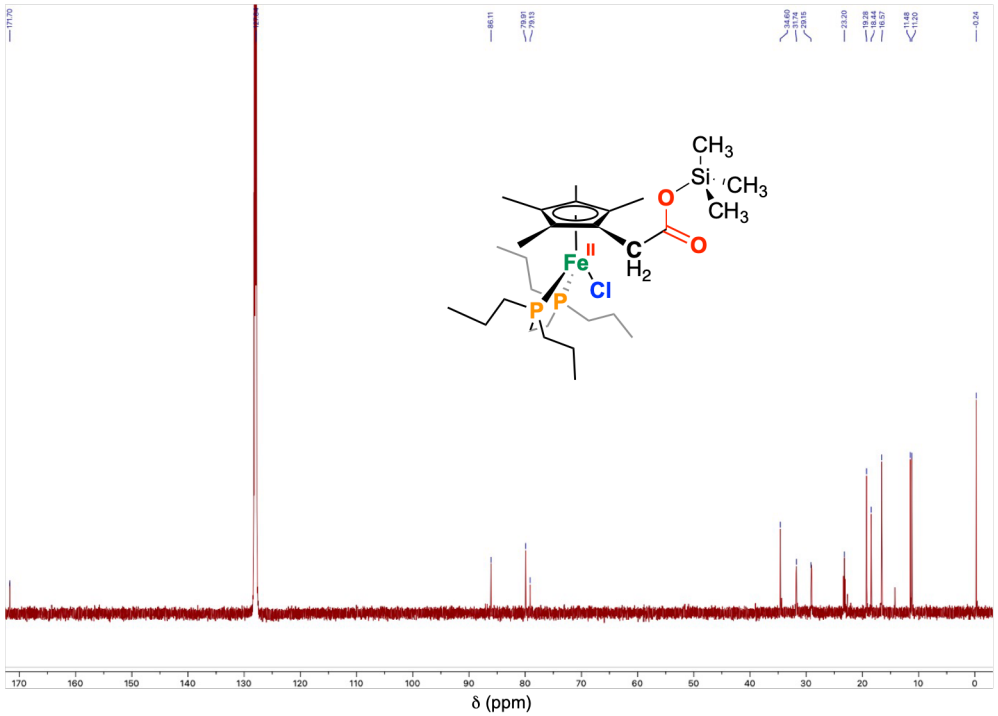

Figure S5: 2, FTIR (benzene film). υ = 1716 cm^{-1} (C=O).

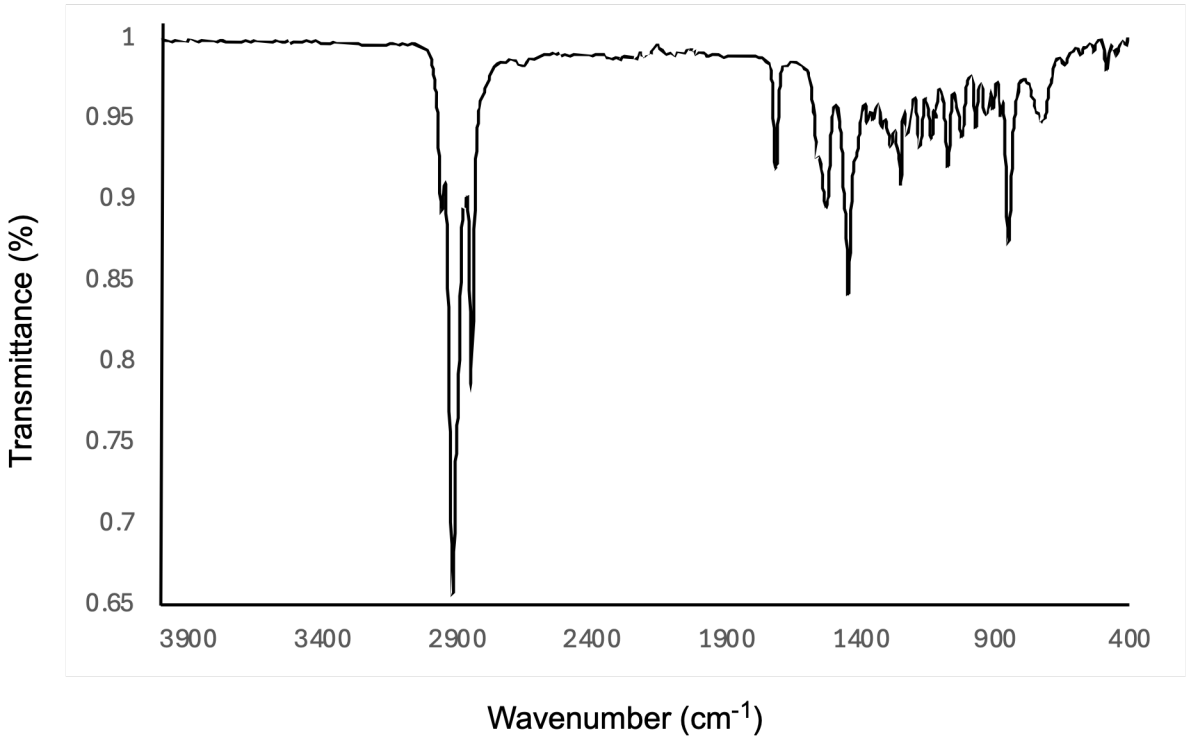

Figure S6: 3, $^{31}P\{^{1}H\}$ NMR, C_6D_6, 162 MHz, 298 K.

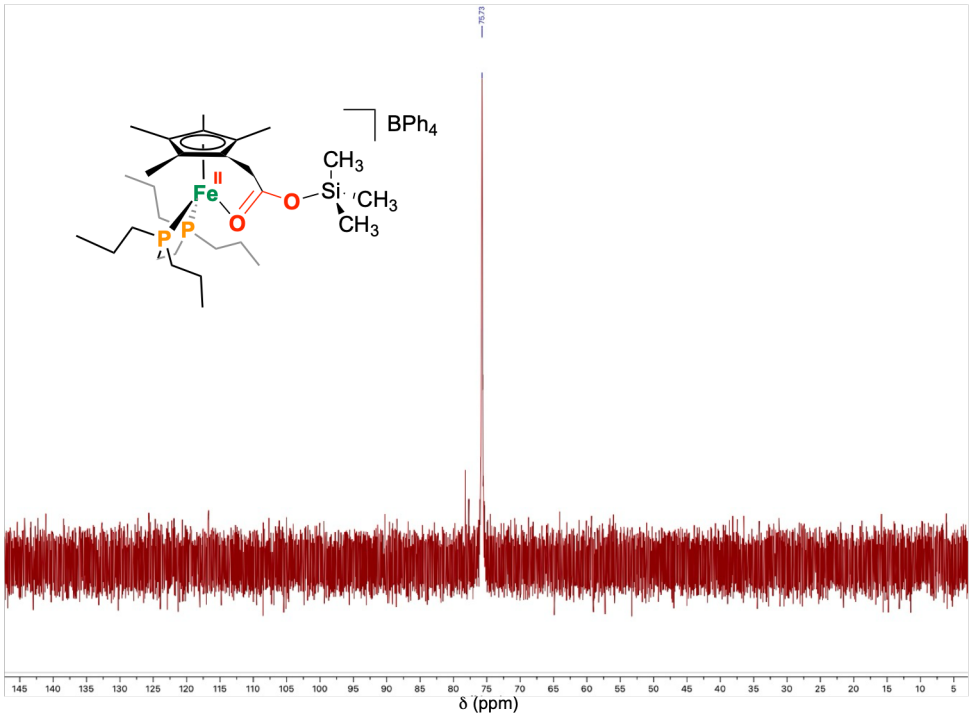

Figure S7: 3, $^{31}P\{^{1}H\}$ VT NMR, THF−H_8, 243 MHz, 298 K. (25, 0, −25, −50, −75 °C)

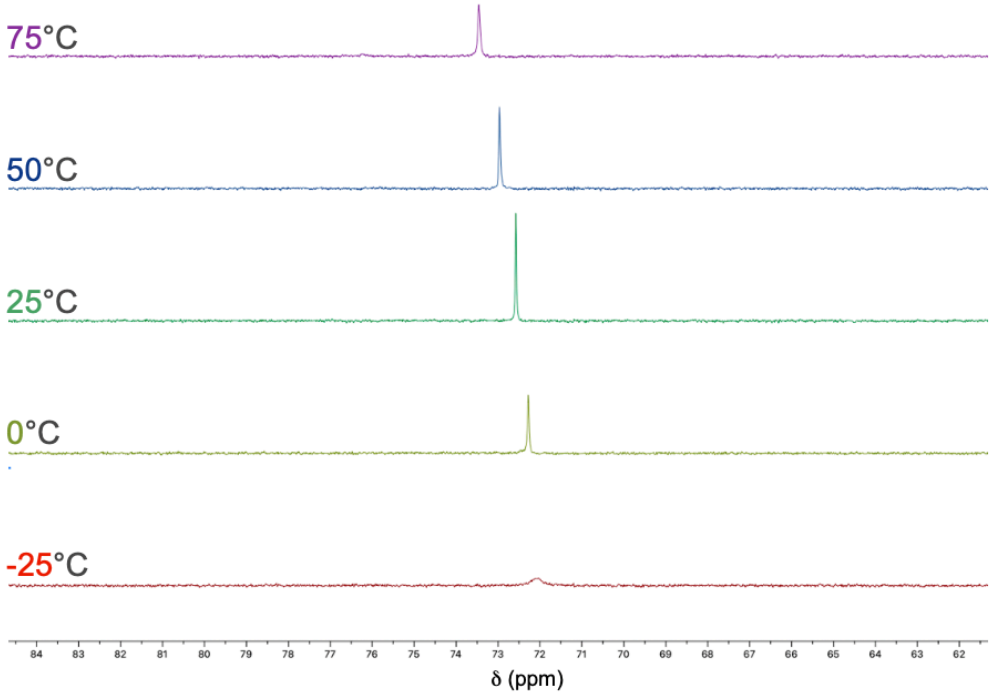

Figure S8: 3, FTIR (ATR, THF Film) shows no $\upsilon(N_2)$ stretch.

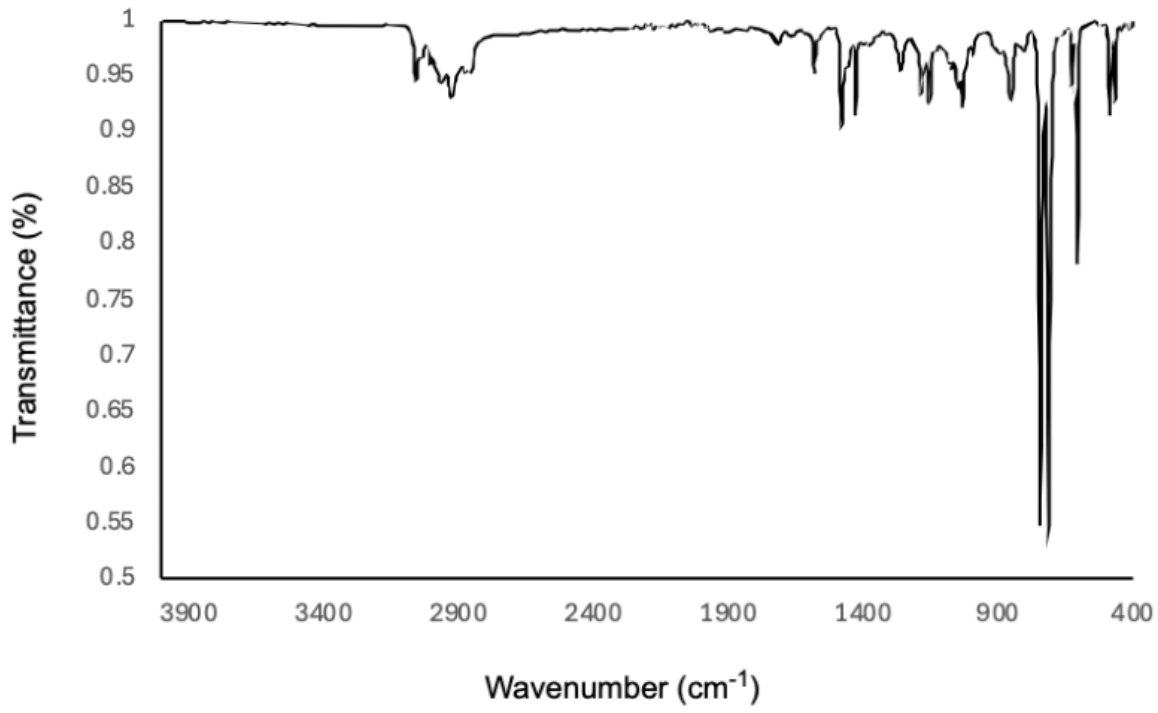

Figure S9: 4, ^{1}H NMR, THF−d_8, 400 MHz, 298 K at t = 5 min. (*=unknown impurity)

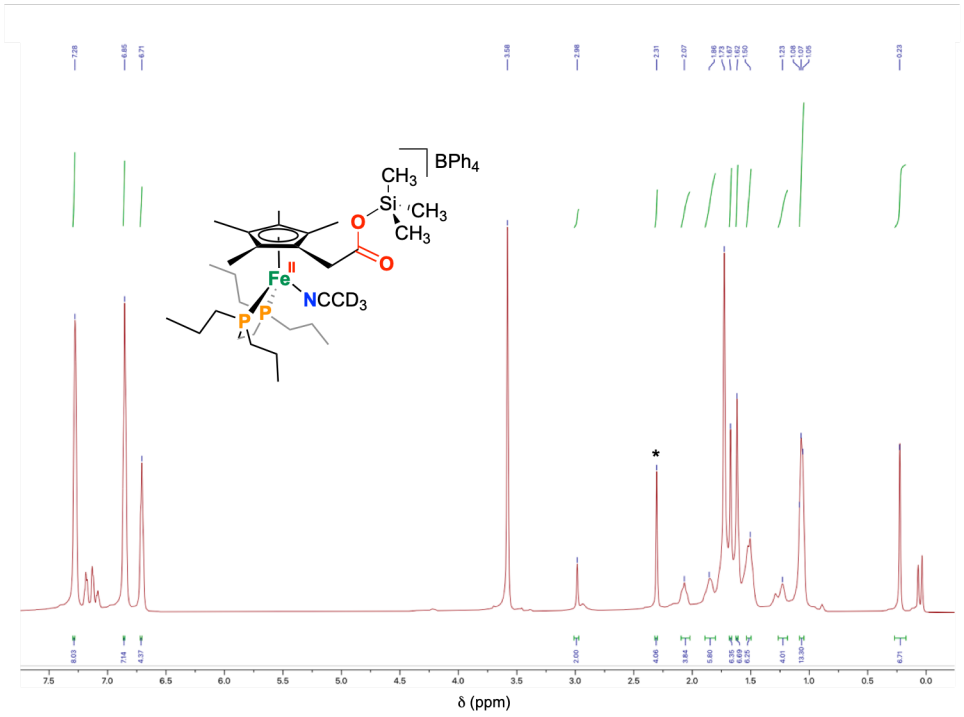

Figure S10: 4, $^{31}P\{^{1}H\}$ NMR, THF−d_8, 162 MHz, 298 K at t = 5 min.

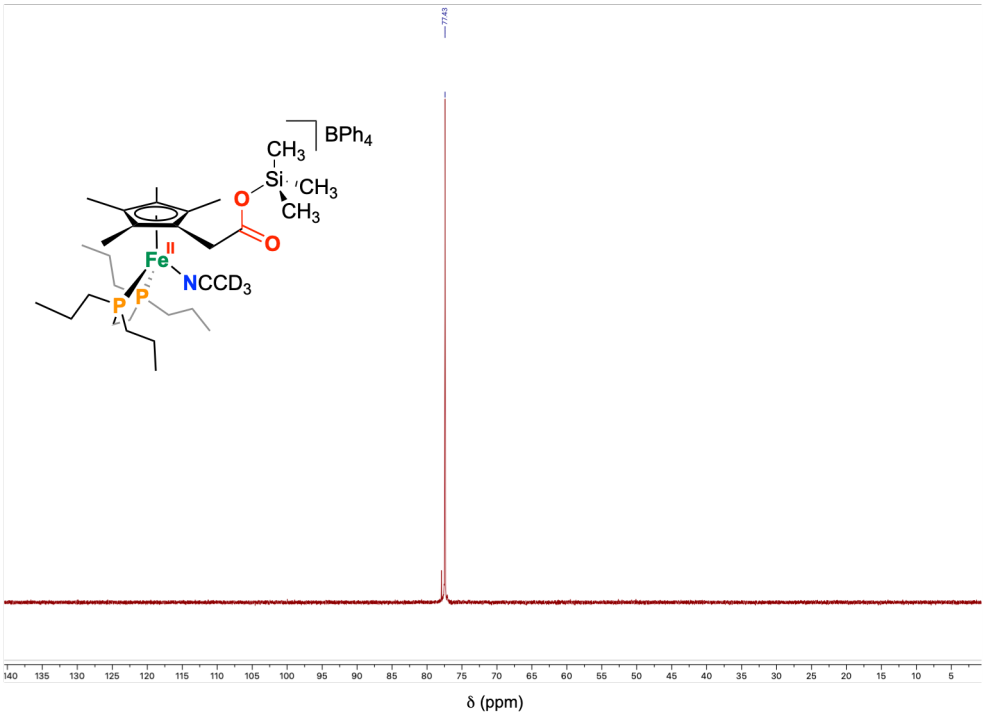

Figure S11: 4, ^{11}B NMR, THF−d_8, 128 MHz, 298 K at t = 5 min.

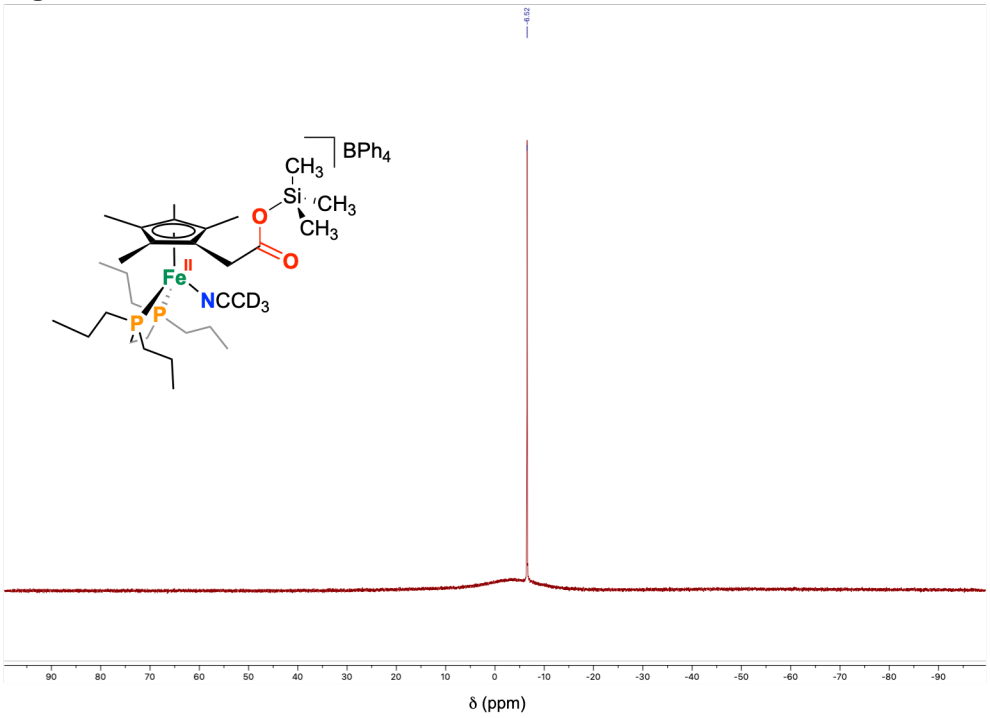

Figure S12: 4, ^{1}H NMR, THF−d_8, 400 MHz, 298 K at t = 12 h showing decomposition to **5**.

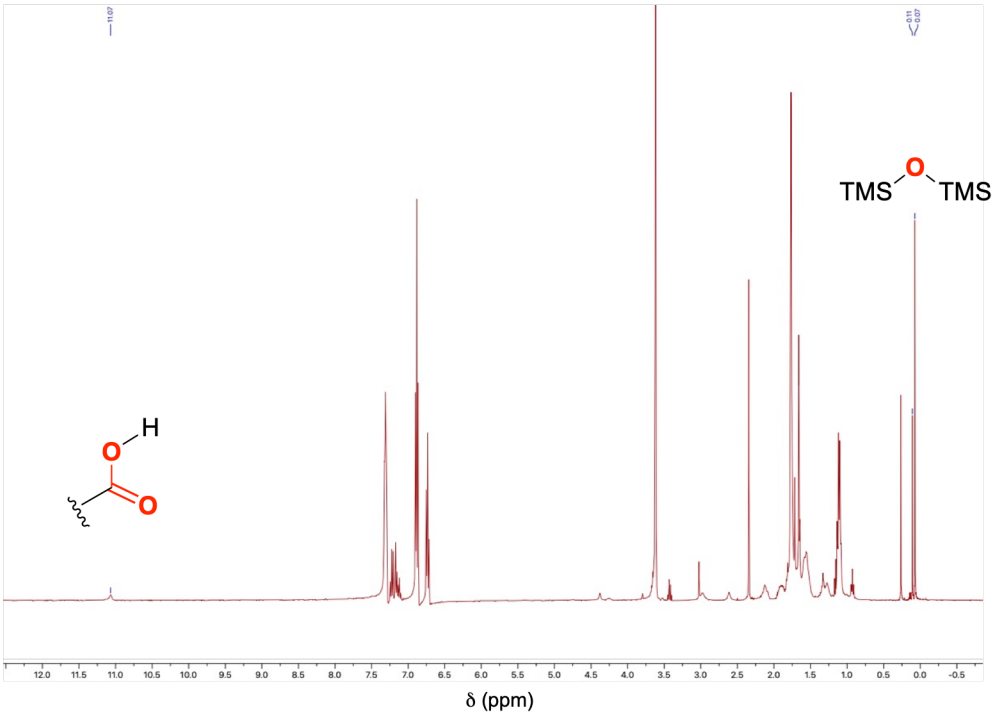

Figure S13: 4, $^{31}P\{^{1}H\}$ NMR, THF−d_8, 162 MHz, 298 K at t = 12 h showing decomposition to **5**.

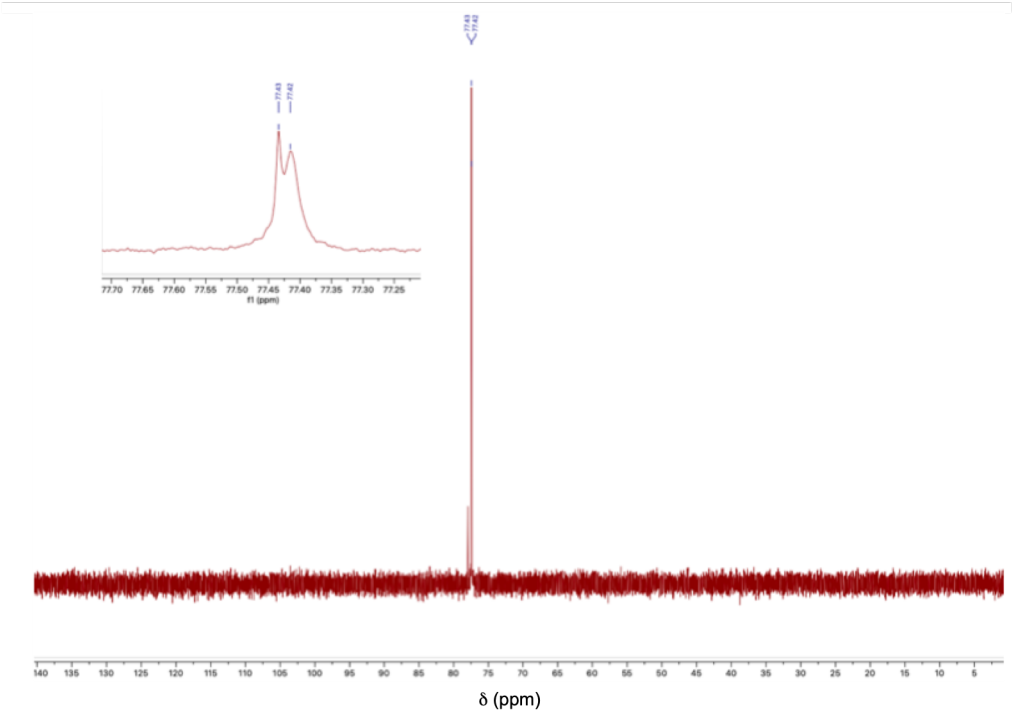

Figure S14: 4, ^{1}H NMR, THF−d_8, 400 MHz, 298 K at t = 5 min (bottom) 12 h (top).

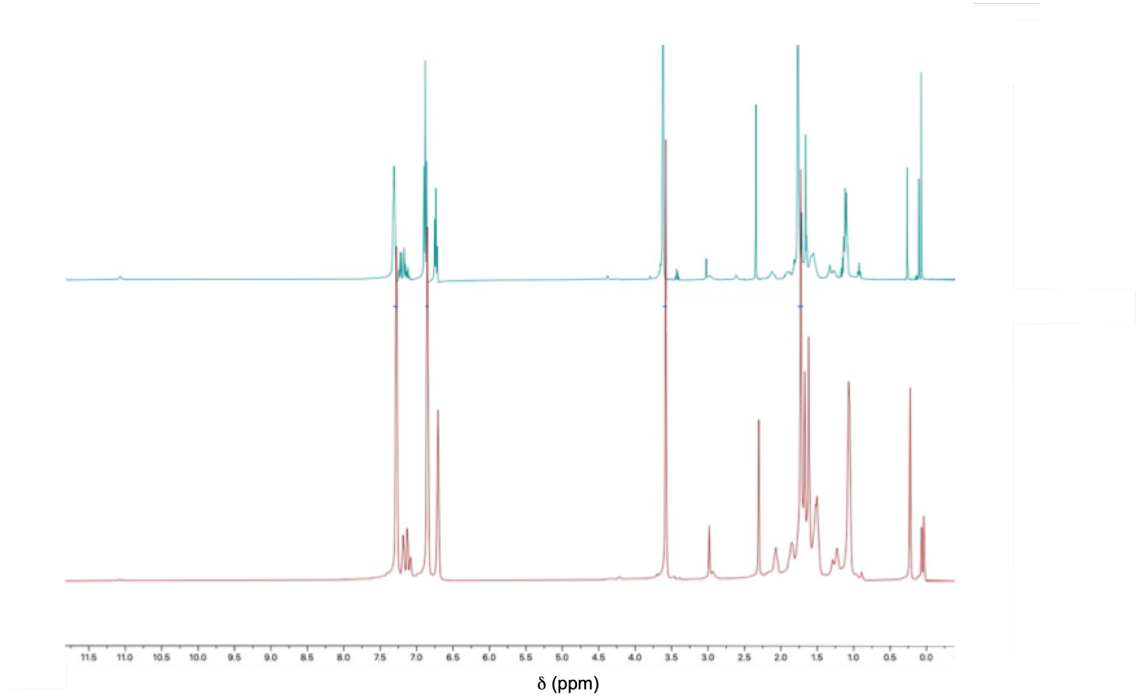

Figure S15: 4, $^{31}P\{^{1}H\}$ NMR, THF−d_8, 162 MHz, 298 K at t = 5 min (bottom) 12 h (top).

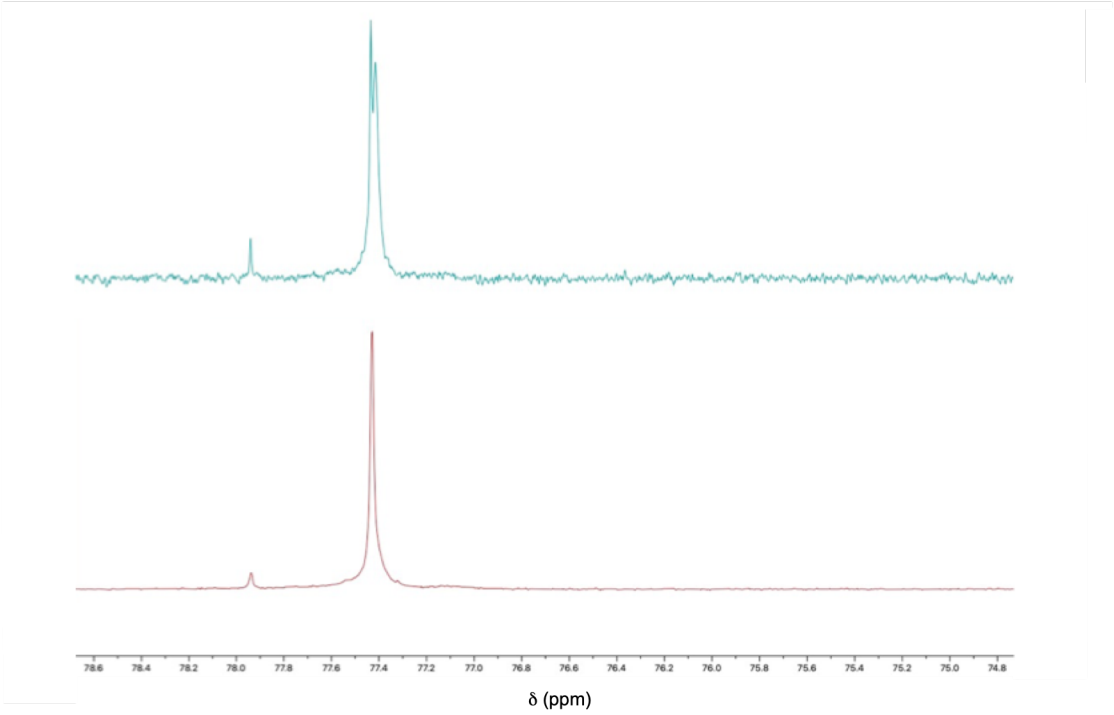

Figure S16: 4, FTIR (ATR, Acetonitrile film): υ = 2243 cm^{-1} (C≡N).

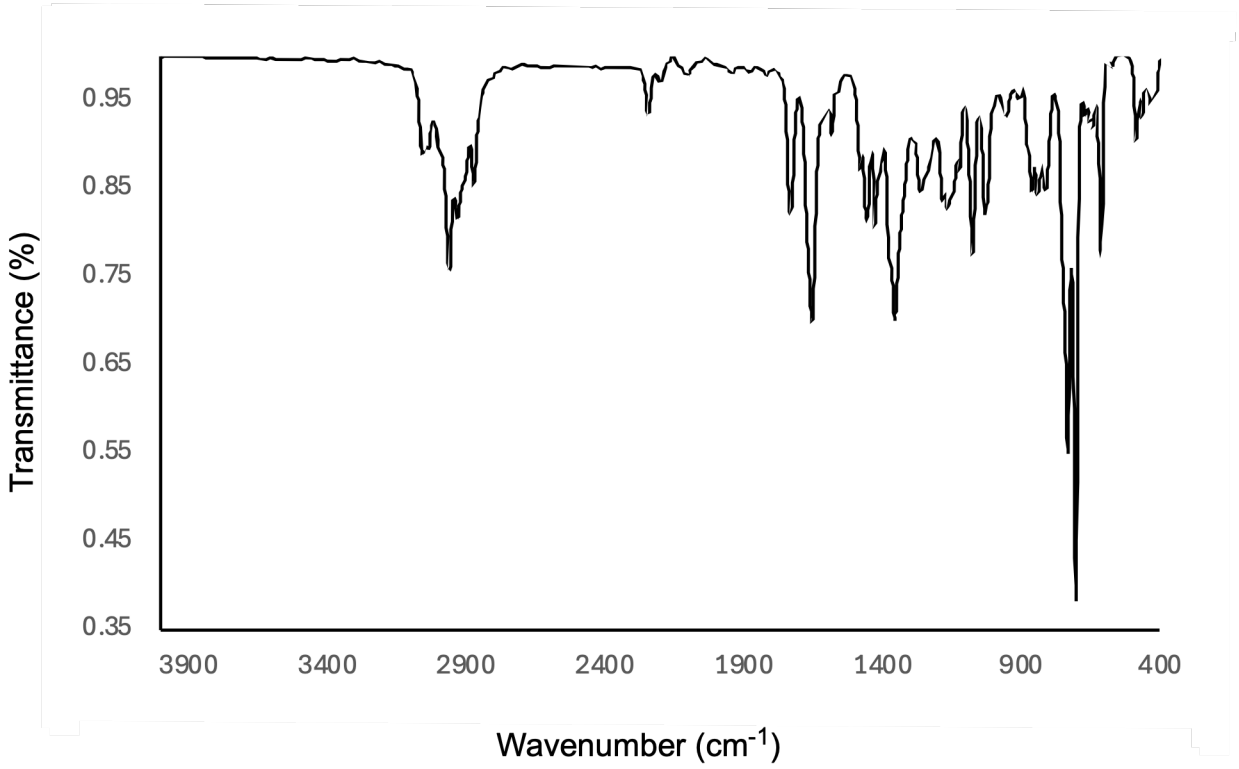

Figure S17: Reaction of **2** with 5 equiv. $HBCy_2$, ^1H NMR, C_6D_6, 400 MHz, 298 K.

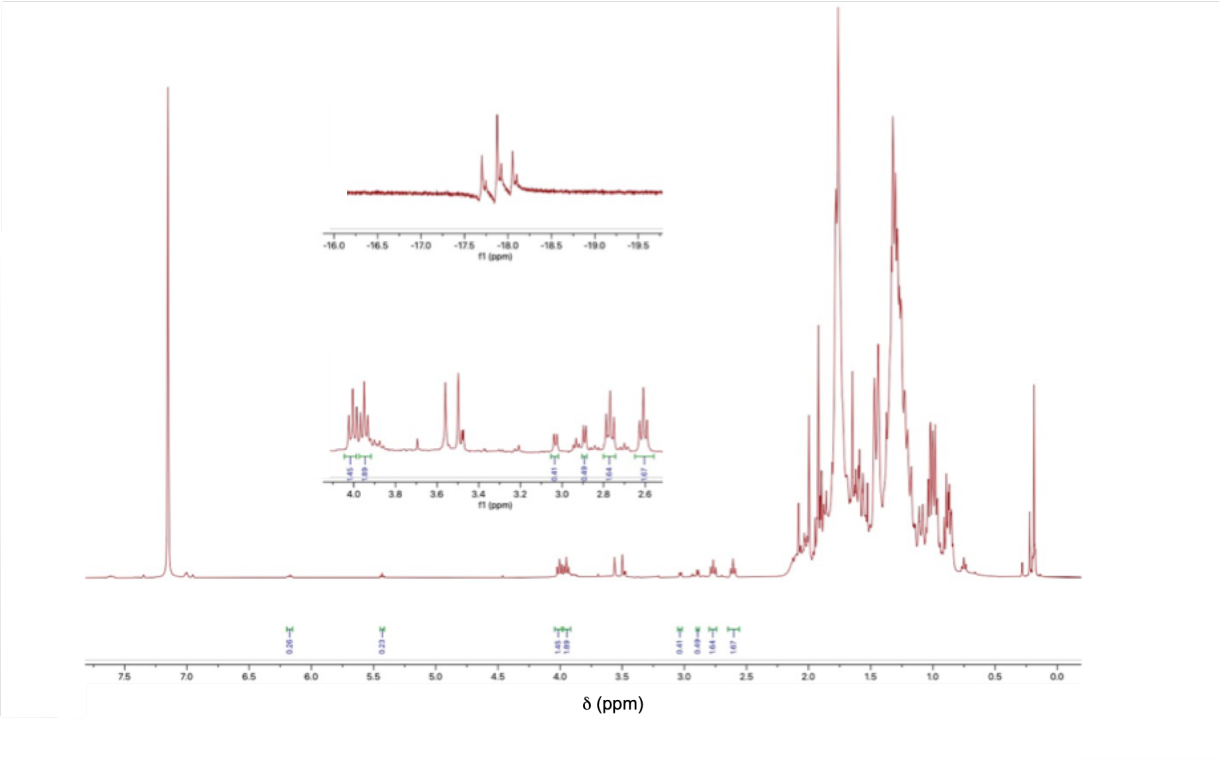

Figure S18: ^1H 1D TOCSY NMR from Figure S17, C_6D_6, 600 MHz, 298 K (Irradiation at δ_H = 3.95).

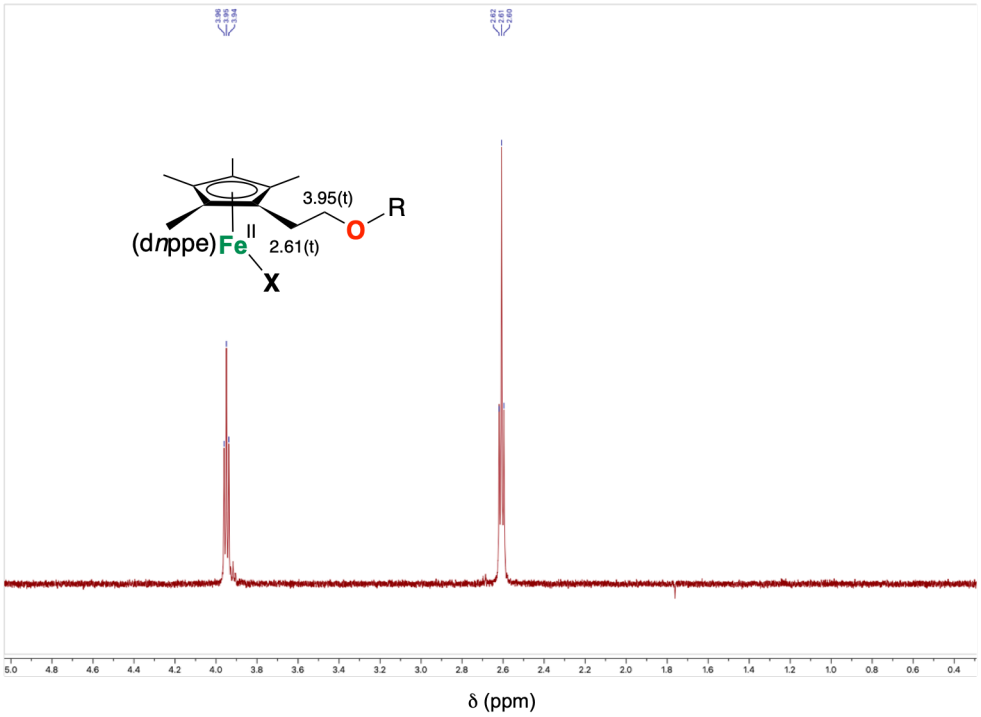

Figure S19: ^{1}H 1D TOCSY NMR from Figure S17, C_6D_6, 600 MHz, 298 K (Irradiation at δ_H = 5.43).

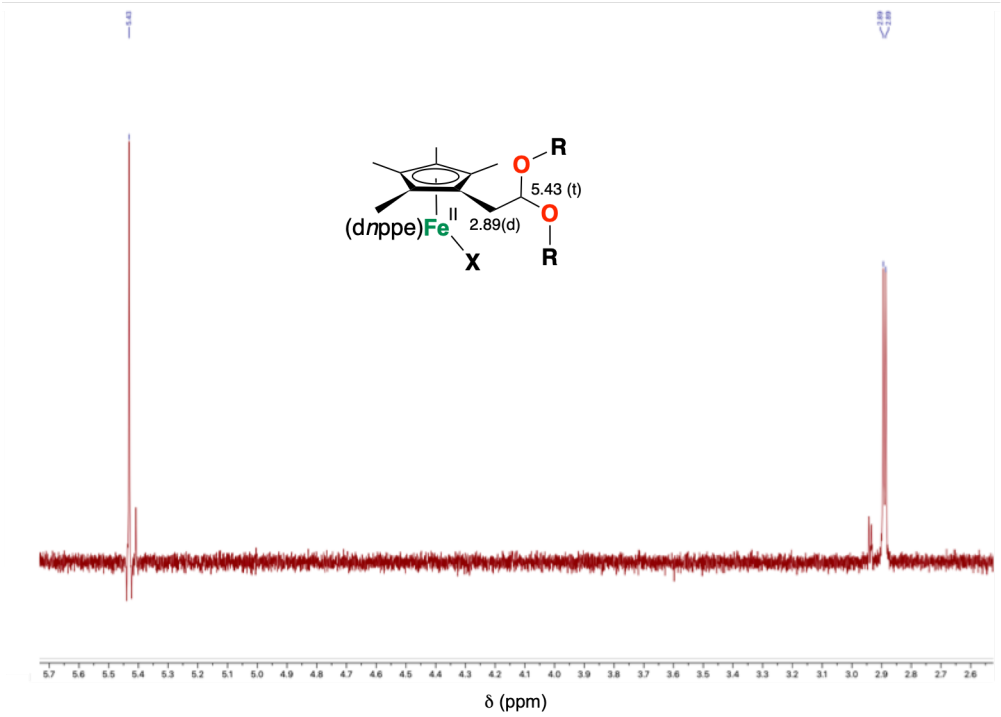

Figure S20: ^{1}H 1D TOCSY NMR from Figure S17, C_6D_6, 600 MHz, 298 K (Irradiation at δ_H = 6.17 ppm).

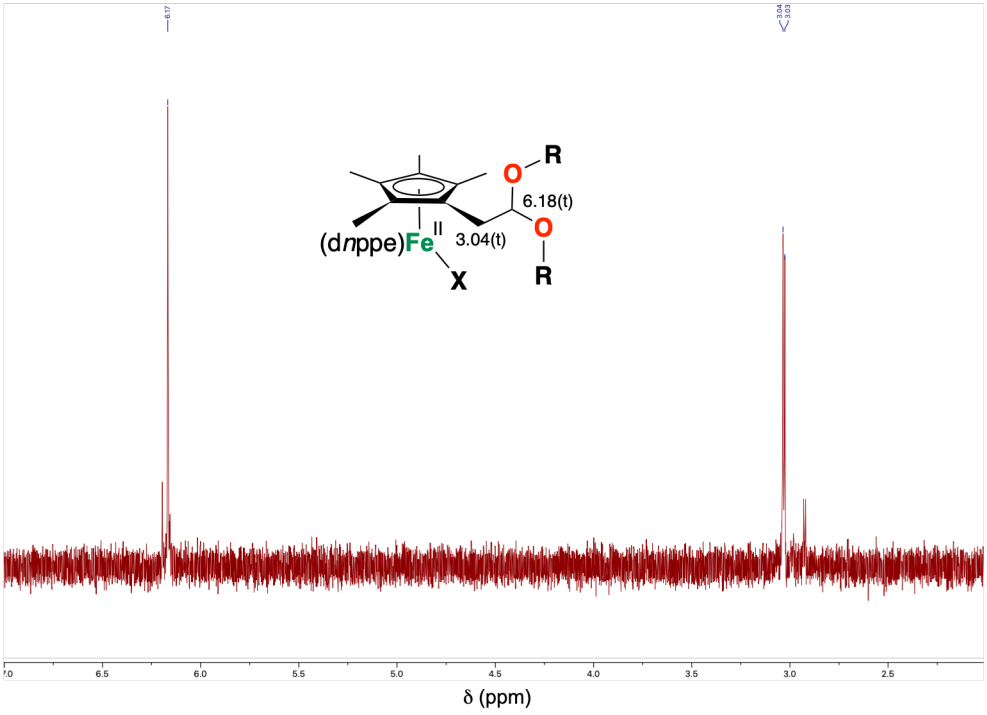

Figure S21: Reaction of **2** with 5 equiv. $HBCy_2$, $^{31}P\{^1H\}$ NMR, C_6D_6, 162 MHz, 298 K.

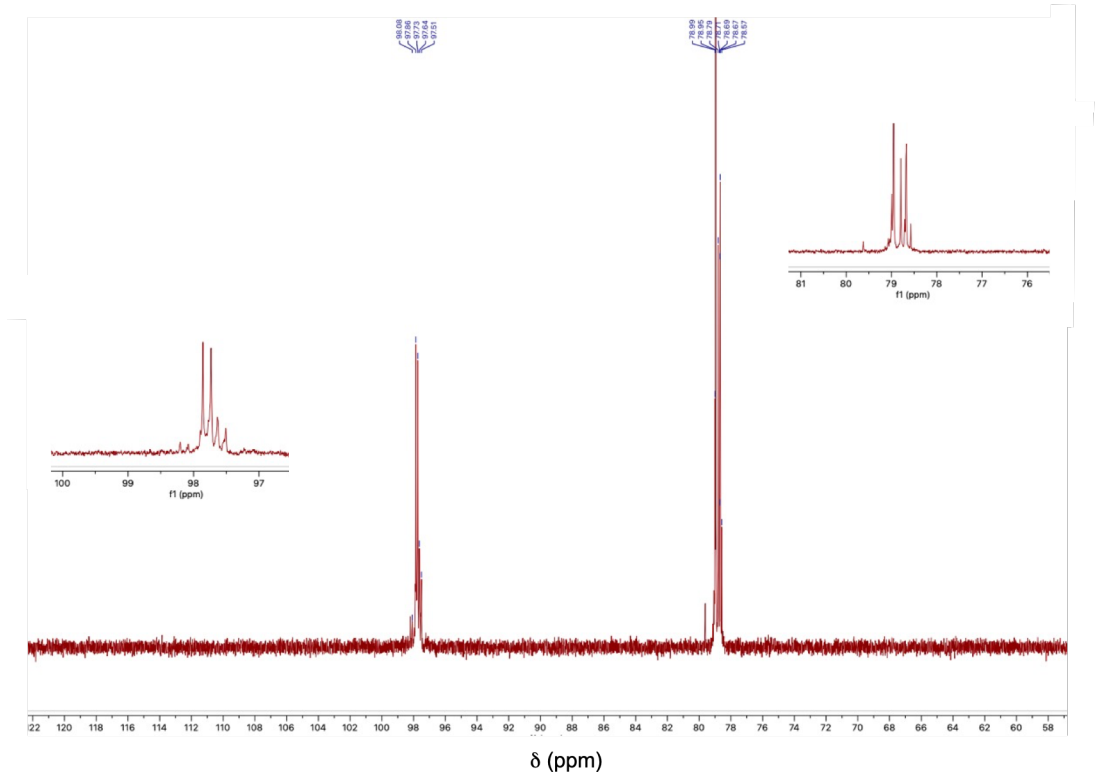

Figure S22: Reaction of **2** with 5 equiv. $HBCy_2$, ^{11}B NMR, C_6D_6, 128 MHz, 298 K. δ_B = 45−55 ppm (RO_2B-R).

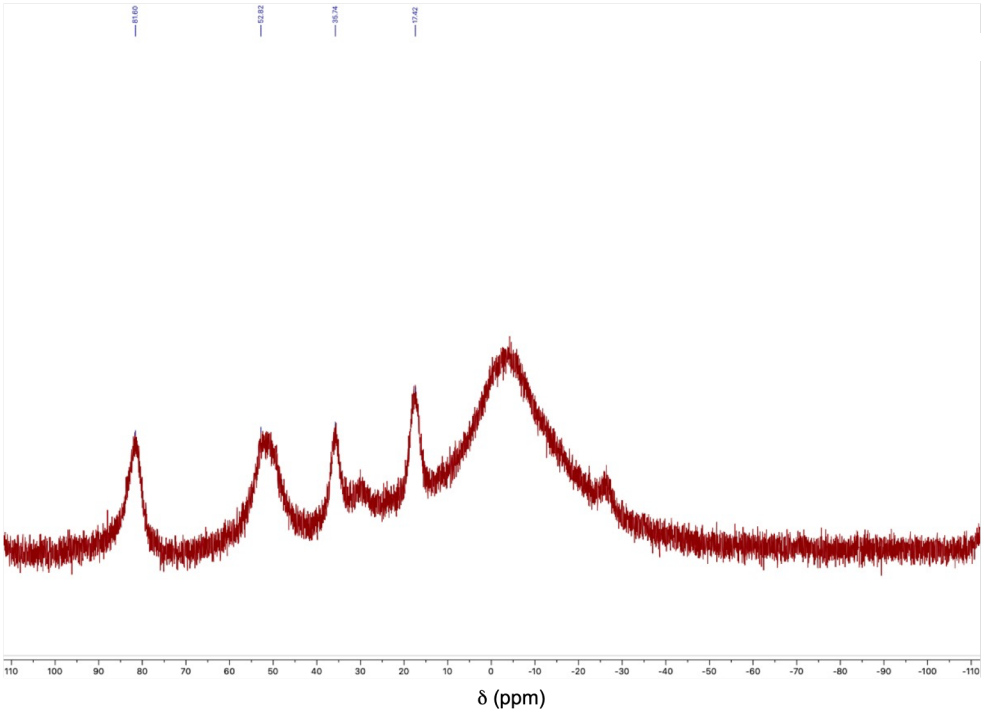

Figure S23: Reaction of **2** with 5 equiv. $HBCy_2$, ^1H, ^1H COSY NMR, C_6D_6, 600 MHz, 298 K showing triplet and acetal cross peaks.

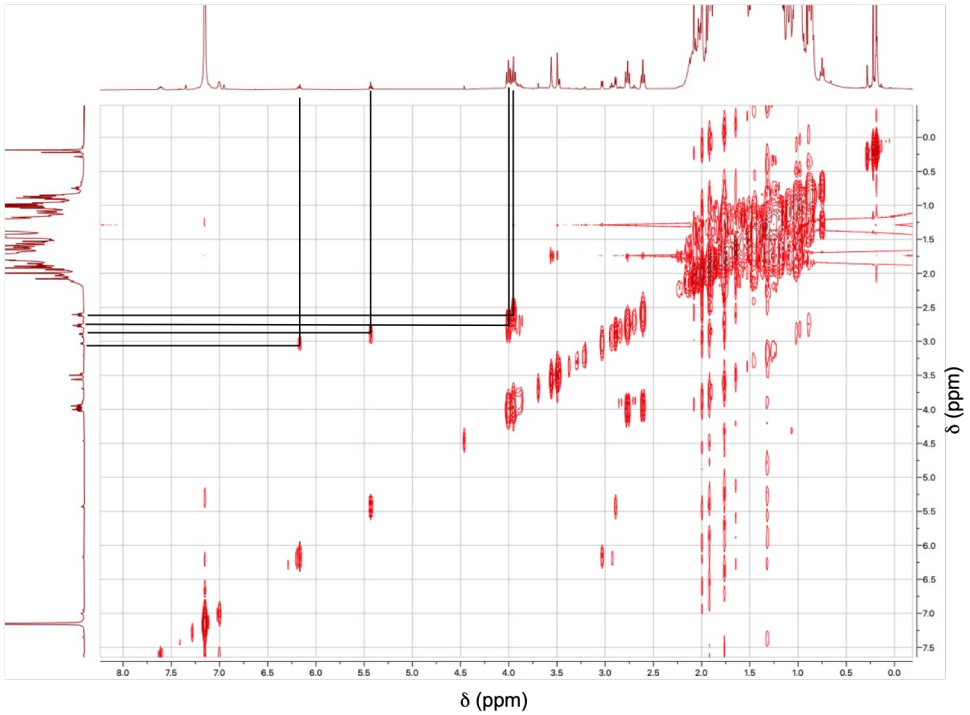

Figure S24: Reaction of **2** with 5 equiv. $HBCy_2$, ^1H,^{13}C HSQC NMR, C_6D_6, 600 MHz, 298 K.

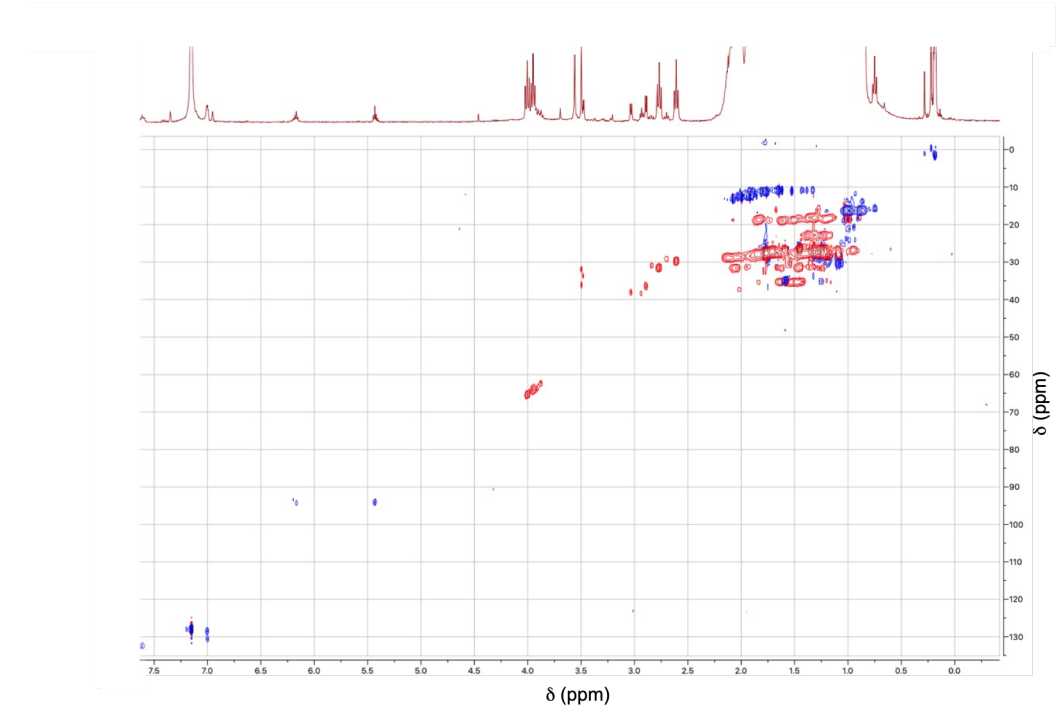

Figure S25: Reaction of **2** with 5 equiv. $HBCy_2$, FT− IR, Benzene Film, 298K. Confirms C=O reduction (absence of a signal 1500−1800 cm^{-1}).

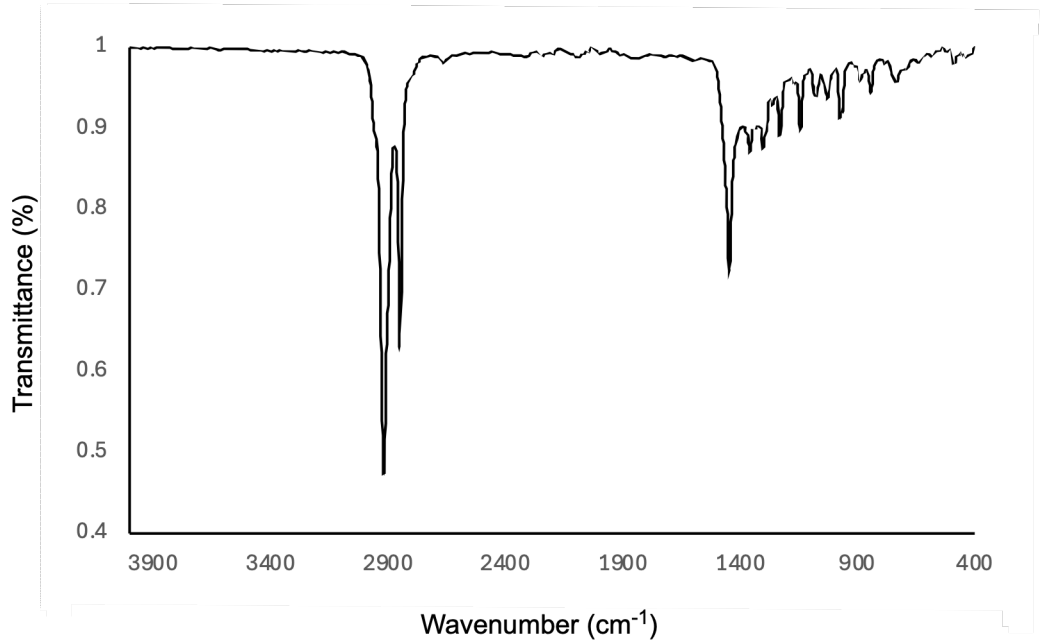

Figure S26: Reaction of **2** with 5 equiv. $HBCy_2$, ^1H NMR, C_6D_6, 400 MHz, 298 K. Reactivity of reduction reaction mixture with $NaBPh_4$ (hexane soluble portion).

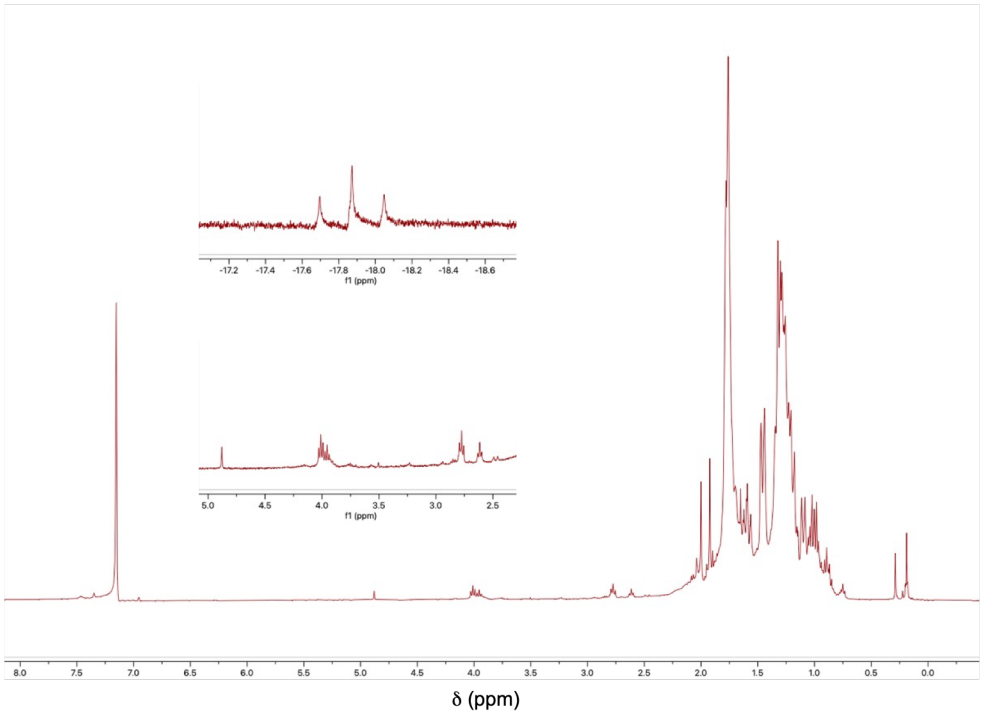

Figure S27: Reaction of **2** with 5 equiv. $HBCy_2$, $^{31}P\{^1H\}$ NMR, C_6D_6, 162 MHz, 298 K. Reactivity of reduction reaction mixture with $NaBPh_4$ (hexane soluble portion).

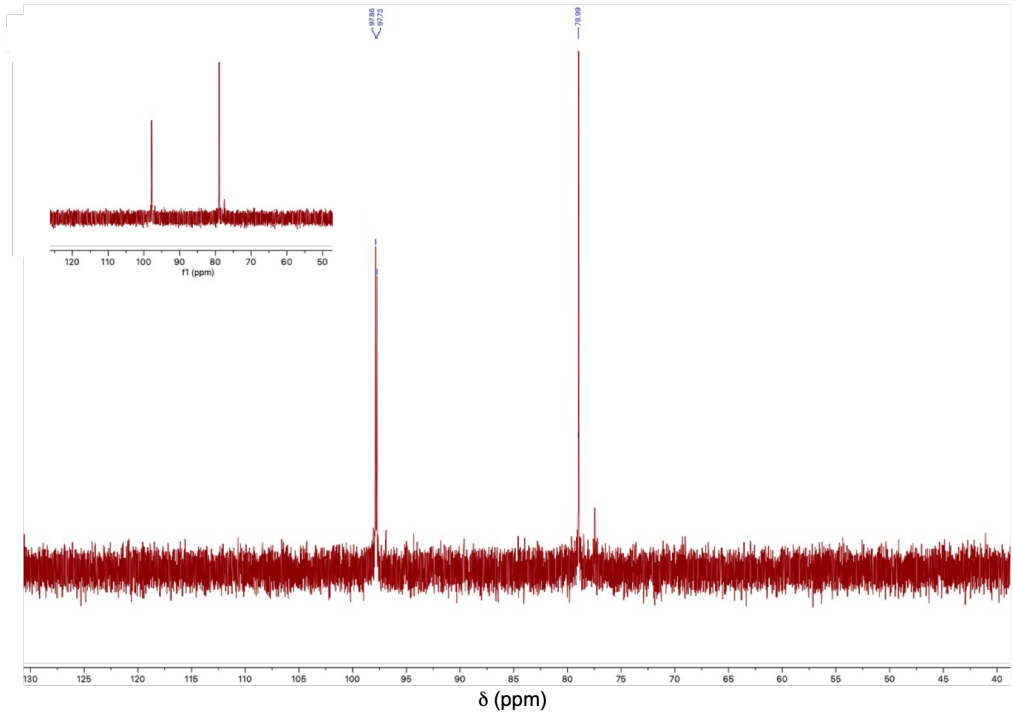

Figure S28: Reaction of **2** with 5 equiv. $HBCy_2$, ^{11}B NMR, C_6D_6, 128 MHz, 298 K. Reactivity of reduction reaction mixture with $NaBPh_4$ (hexane soluble portion).

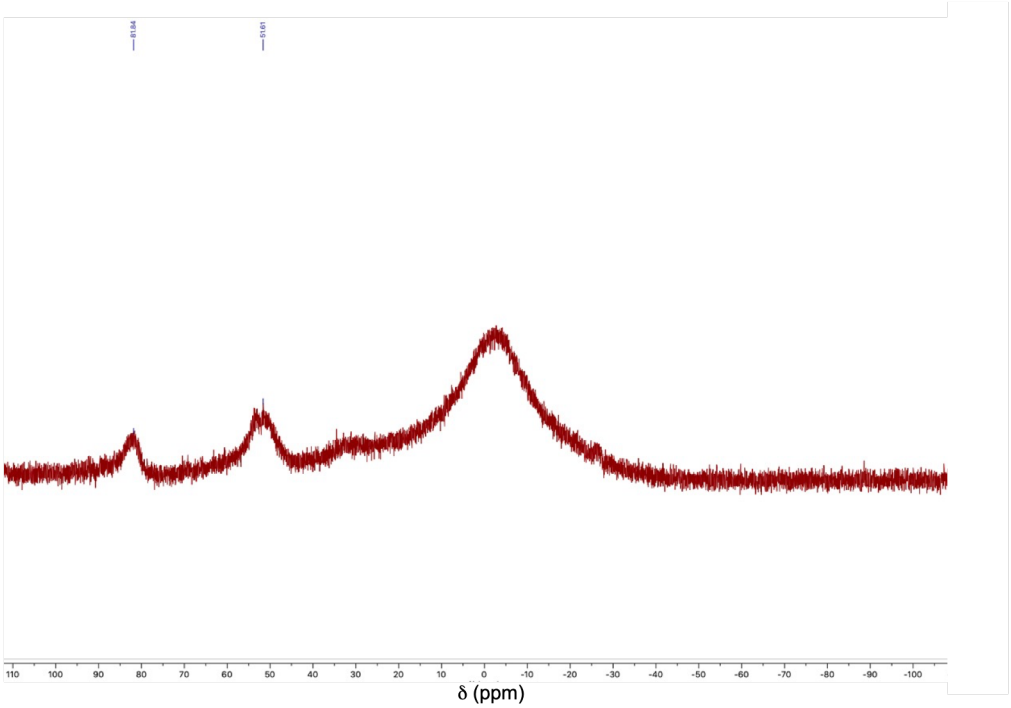

Figure S29: ^{1}H NMR, C_6D_6, 400 MHz, 298K. Reactivity of reduction reaction mixture with $NaBPh_4$ (hexane soluble portion) (bottom) stacked with pre−cleaning (top).

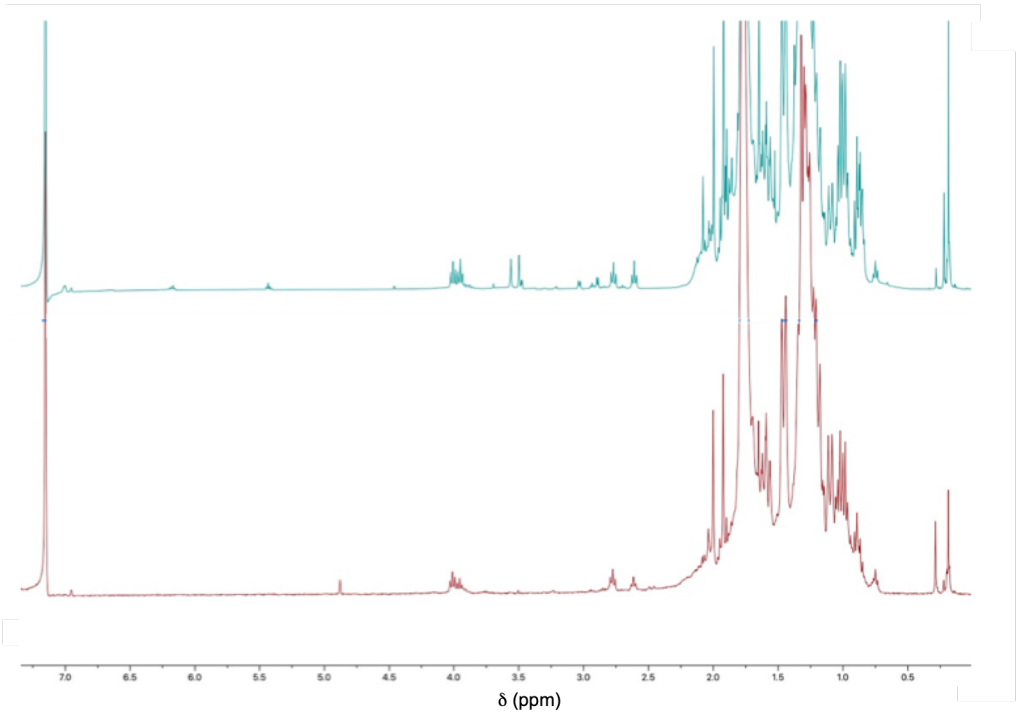

Figure S30: $^{31}P\{^{1}H\}$ NMR, C_6D_6, 162 MHz, 298 K. Reactivity of reduction reaction mixture with $NaBPh_4$ (hexane soluble portion) (bottom) stacked with pre−cleaning (top).

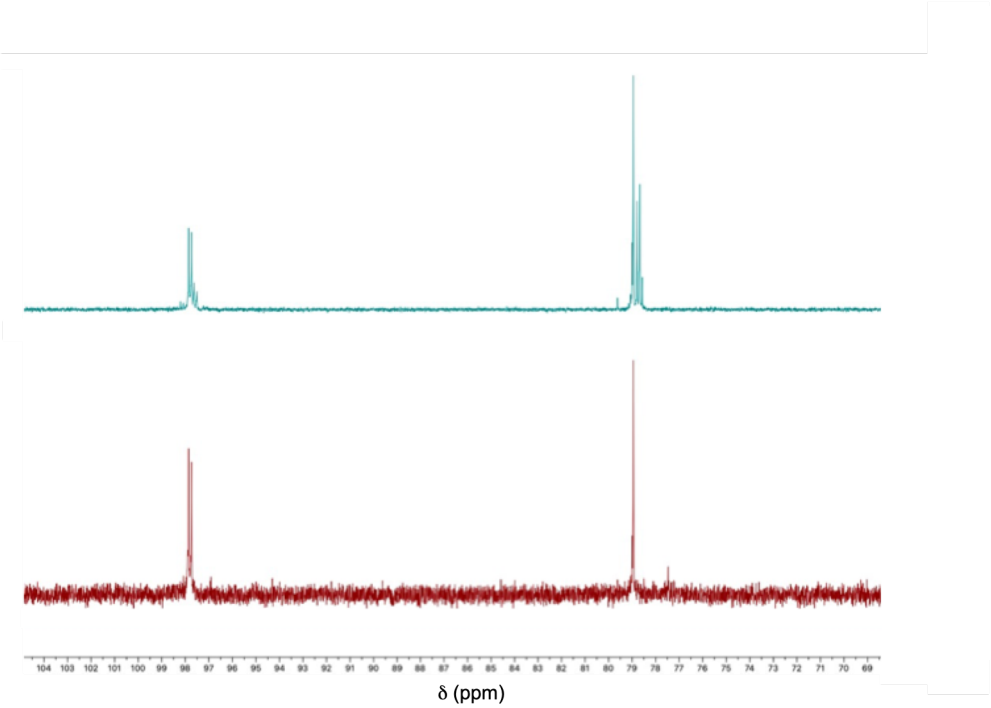

Figure S31: ^{11}B NMR, C_6D_6, 128 MHz, 298 K. Reactivity of reduction reaction mixture with $NaBPh_4$ (hexane soluble portion) (bottom) stacked with pre−cleaning (top).

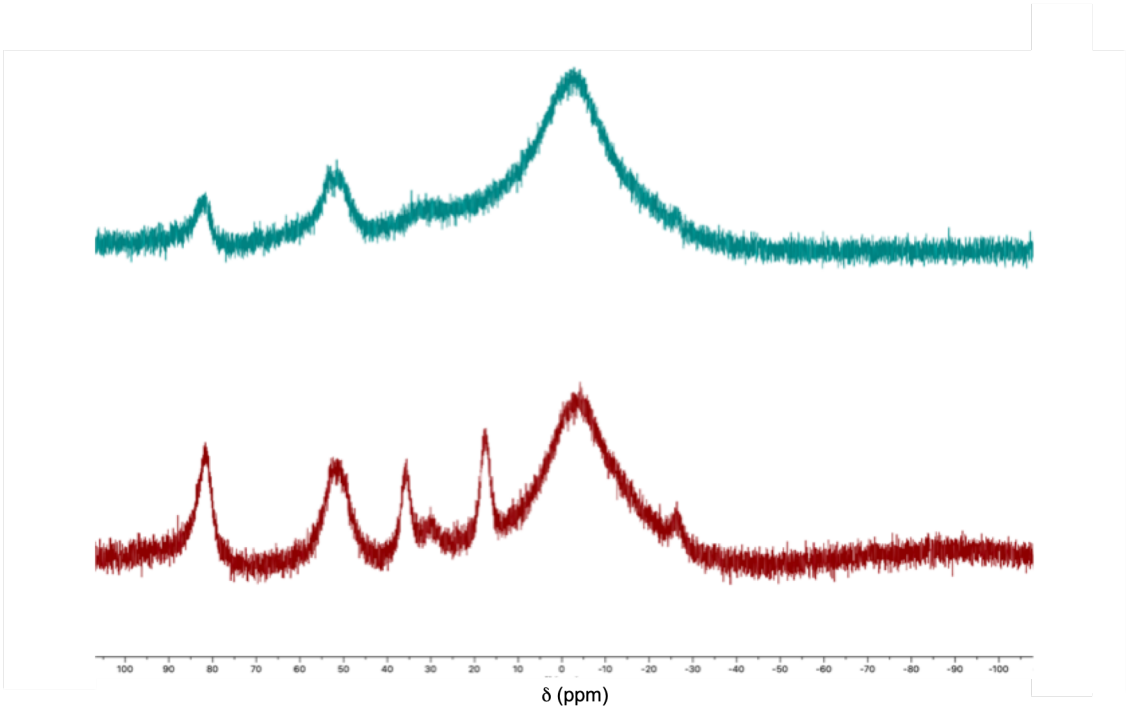

2. Mass spectrometry:

Figure S32: 2, LIFDI−HRMS: $C_{28}H_{55}ClFeO_2P_2Si$ ($[M]^+$) (604.2485, calculated); (604.2474, observed).

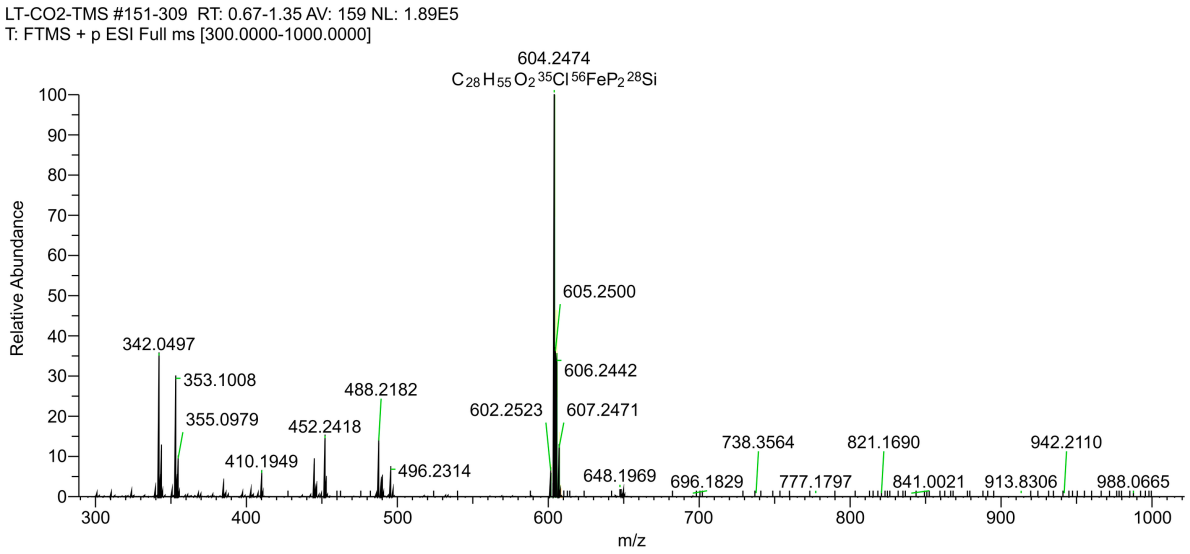

Figure S33: 2, LIFDI−HRMS: $C_{28}H_{55}ClFeO_2P_2Si$ ($[M]^+$) (604.2485, calculated); (604.2474, observed). Isotope pattern.

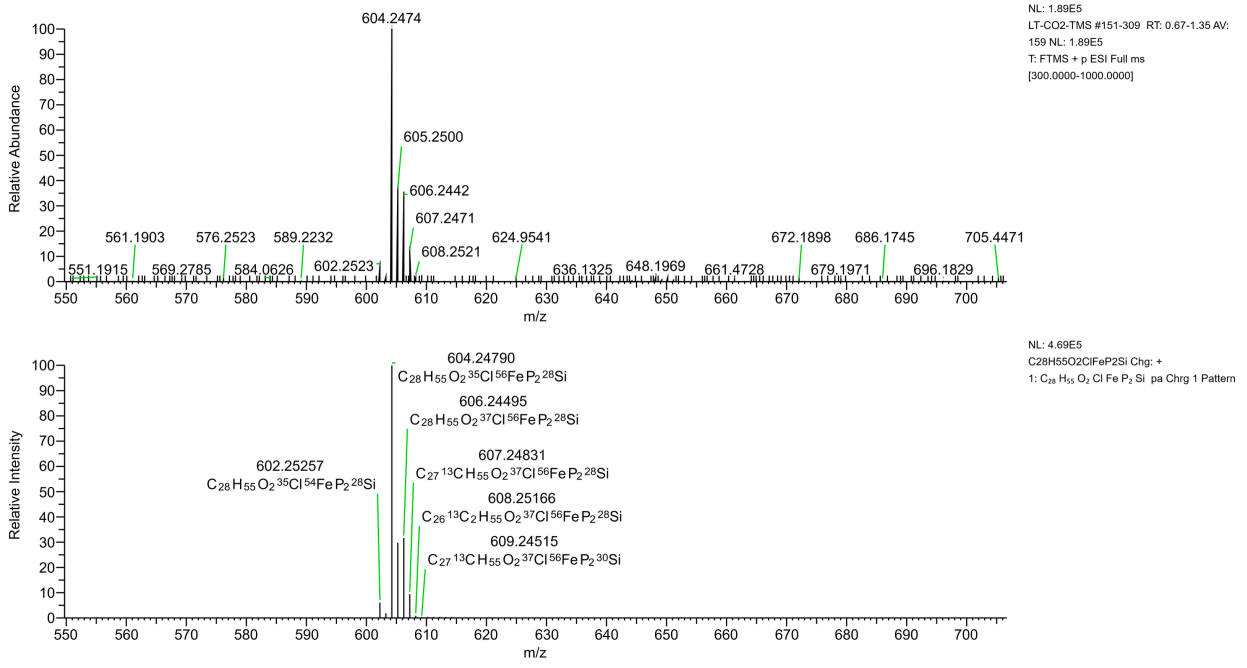

Figure S34: LIFDI−HRMS for reduction reaction mixture of **2** + 5 equiv. $HBCy_2$.

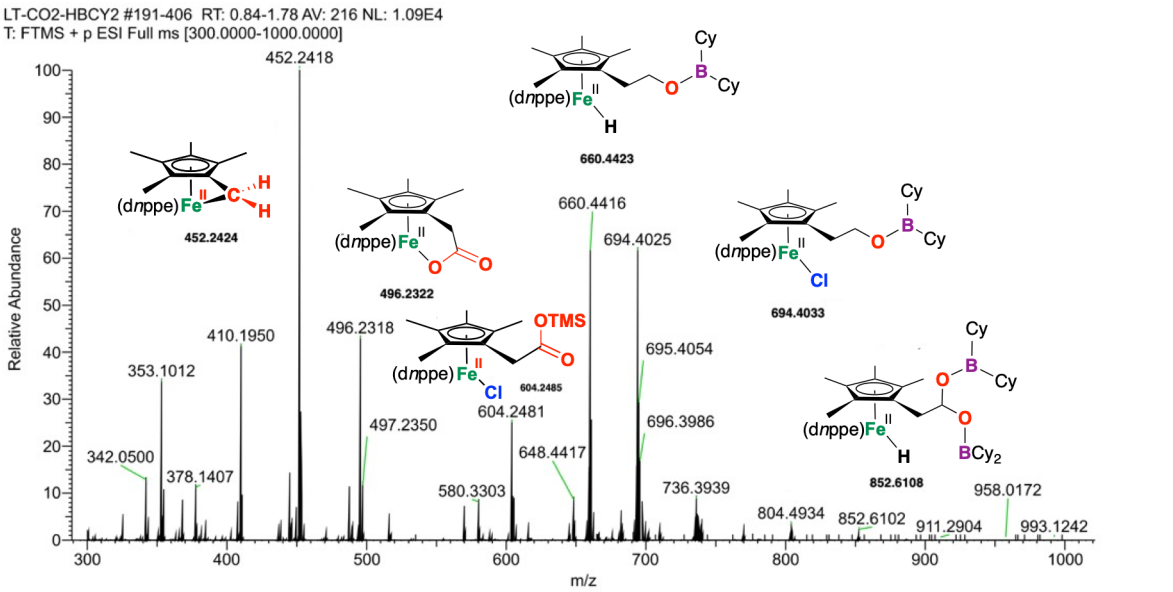

Figure S35: ESI(+)−MS $[\mathbf{5}-H]^+$ $C_{25}H_{46}FeO_2P_2$ (496.232, calculated); (496.231, observed).

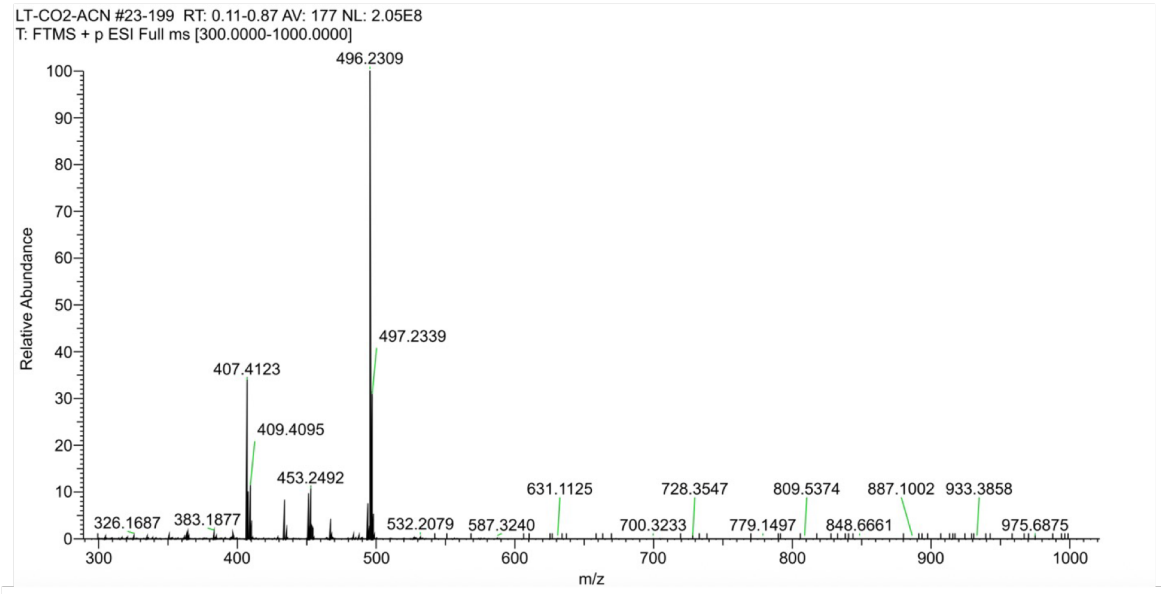

3. Crystallographic details:

CCDC **2575113** contains the supplementary crystallographic data for this paper. These data can be obtained free of charge from The Cambridge Crystallographic Data Centre *via* https://www.ccdc.cam.ac.uk.

Experimental for 2:

Crystal data were collected with Mo*K*α radiation on a Bruker Kappa Axis Apex2 diffractometer at Western University. All crystals were mounted on a MiTeGen loop with a small amount of Paratone N oil. Frame integration, scaling and absorption correction were performed using SAINT and SADABS integrated in Apex4 [1]. The structures were solved with the ShelXT [2] structure solution program using intrinsic phasing and refined with the ShelXL [3] refinement package using least squares on weighted F2 values for all reflections using OLEX2 [4].

Table S1. Crystallographic data for **2**.

Compound	**2**
Empirical Formula	$C_{28}H_{55}ClFeO_2P_2Si$
Formula Weight	605.05
Temperature/K	110.00
Crystal System	Monoclinic
Space group	$P2_1/c$
a/Å	15.276(6)
b/Å	13.058(5)
c/Å	16.903(6)
α/°	90
β/°	104.421(12)
γ/°	90
Volume/Å^3	3266(2)
Z	4
ρ_{calc}g/cm^3	1.231
μ/mm^{-1}	0.701
F(000)	1304.0
Crystal size/mm^3	0.53 x 0.195 x 0.111
Radiation	MoKα (λ = 0.71073)
2Θ range for data collection/°	5.938 to 60.986
Index ranges	$-21 \leq h \leq 21$, $-18 \leq k \leq 18$, $-24 \leq 1 \leq 22$
Reflections collected	160962
Independent reflections	9918 [R_{int} = 0.0981, R_{sigma} = 0.0417]
Data/restraints/parameters	9918/5/326
Goodness−of−fit on F^2	1.028
Final R indexes [I>=2σ (I)]	R_1 = 0.0430, wR_2 = 0.0958
Final R indexes [all data]	R_1 = 0.0775, wR_2 = 0.1158
Largest diff. peal/hole / e Å^3	0.72/−0.90

Where:

$R_1 = \Sigma \mid |F_o| - |F_c| \mid / \Sigma F_o$
$wR_2 = [\ \Sigma(w(F_o^2 - F_c^2)^2) / \Sigma(w F_o^4)\ ]^{½}$
$GOF = [\ \Sigma(w(F_o^2 - F_c^2)^2) / (\text{No. of reflns.} - \text{No. of params.})\ ]^{½}$

4. References:

(1) Bruker (2016). APEX3, SAINT and SADABS. Bruker AXS Inc., Madison, Wisconsin, USA.

(2) Sheldrick, G. M. *Acta Crystallogr. Sect. A* **2015**, *71* (1), 3–8. https://doi.org/10.1107/S2053273314026370.

(3) Sheldrick, G. M. *Acta Crystallogr. Sect. C* **2015**, *71* (1), 3–8. https://doi.org/10.1107/S2053229614024218.

(4) Dolomanov, O. V.; Bourhis, L. J.; Gildea, R. J.; Howard, J. A. K.; Puschmann, H. *J Appl. Crystallogr.* **2009**, *42* (2), 339–341. https://doi.org/10.1107/S0021889808042726.